文章编号:1000-8055(2013)05-1047-10

Experiments of effects of inlet-air distortion on aerodynamic performance in transonic compressor

LI Mao-yi, YUAN Wei, LU Ya-jun, SONG Xi-zhen, LU Li-peng

(National Key Laboratory of Science and Technology on Aero-Engine Aero-thermodynamics, School of Energy and Power Engineering, Beijing University of Aeronautics and Astronautics, Beijing 100191, China)

Abstract: The inlet-air distortion which was caused by high angle-of-attack flight was simulated by plug-board. Experiments were conducted on a transonic axial-flow compressor's rotor at 98% rotating speed. The flow-field characteristics and mechanism of performance degradation were analyzed in detail. The compressor inlet was divided into four sectors at circumference under inlet-air distortion. They were undistorted sector, transition sector A where the rotor was rotating into the distortion sector, distorted sector and transition sector B where the rotor was rotating out of the distortion sector. The experimental results show that compared with undistorted sector, there is a subsonic flow in transition sector A, so the pressure ratio is decreased by a large margin in this sector. However, the shock wave is enhanced in distortion sector and transition sector B, and thus the pressure ratio increases in these sectors. Because of the different works at circumference, the phase angle of total pressure changes 90° when the inlet total pressure distortion passes through compressor rotor. In addition, the frequency and amplitude of disturbances in front of the rotor strengthenes under inlet distortion, so the unstable flow would take place in advance. In addition, the position of stall inception is in one of the transition sectors.

Key words: plugboard simulator; inlet-air distortion; transonic axial-flow compressor; shock wave; disturbance

CLC number: V231 **Document code**: A

Nomenclature

π^*	total pressure ratio	ΔM_s	increment of stall margin (%)
η_r^*	relative efficiency	D	inner diameter of casing (mm)
$\eta_{r\_peak}^*$	relative peak efficiency	m_r	relative flowrate
$\Delta\eta_{r\_peak}^*$	increment of relative peak efficiency	V	measured voltage in neal time/V
M_s	stall magin(%)	V_m	mean voltage/V

Introduction

Early design and analysis of turbomachine are carried out under the assumption of uniform inlet. With the continuous improvement of the performance requirements to the plane, the advanced combat aircraft must have the ability of high maneuverability and high angle-of-attack to fly, which makes the inlet parameters become nonuniform, and the limitation of uniform inlet

Received: 2012-05-29

URL: http://www.cnki.net/kcms/detail/11.2297.V.20130508.0949.201305.1047_012.html

Foundation item: National Natural Science Foundation of China (50906001)

E-mail: limaoyi_beihang@163.com

assumption is revealed gradually. In the early 1950's, Harry et al.[1] and Malker et al.[2] used distortion screen to simulate inlet-air distortion of engine, and the effect of aerodynamic performance and stability was investigated on an engine by experiment. The experimental results showed that the aerodynamic performances of engine were worsened seriously. Through analyzing the effect of inlet-air distortion on tip leakage vortex and blade aerodynamic load, the flow factors that the inlet-air distortion influences compressor aerodynamic performance and stability were explored by domestic and foreign experts[3-4]. The effect of flow structure on transonic compressor's rotor[5] was analyzed deeply by Hah et al. The experimental results showed that the strong pulse was produced at the tip passage, and the range reached 20% blade chord; unsteady shock waves interacted on boundary layer of blade strongly when the rotor blades swept distorted low pressure area under transonic condition, which led to flow blockage area increasing observably. In order to predict the stability of compressor under inlet-air distortion, the researchers developed a variety of theoretical prediction models including parallel compressor model[6-7], linear model[8], actuator disk and semi-actuator disk model and H&G model[9]. With the continuous improvement of computer technology, 3-D numerical simulation is widely applied in the inlet-air distortion research. Annulus numerical simulation that distorted parameters transfer along compressor was carried out on a single stage and a 3-stage compressor, respectively[10-11]. But there is still much work which needs to be done in order to further understand the mechanism of inlet-air distortion. For example, when the combat aircraft flies in high angle-of-attack, how will the shock wave structure of transonic compressor be changed? And when the total pressure distortion passes the transonic compressor, how will its phase change? And where is the position of the stall inception under inlet-air distortion? And what is the mechanism that the transonic compressor performance decreases? To solve these problems, the flow-field of inlet-air distortion which is caused by high angle-of-attack flight was simulated by setting up a plugboard at the inlet of transonic compressor, and the mechanism that the inlet-air distortion influences the flow-field and performance on transonic compressor was investigated by experiment in detail.

1 Transonic axial-flow compressor test rig and test scheme

Schematic of the present test rig is shown in Fig. 1. The design parameters of the tested compressor is shown in Table 1.

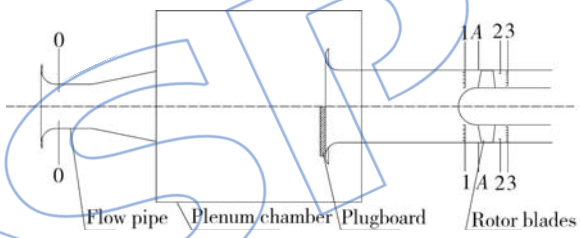

0-0 flow rate static pressure holes; 1-1 inlet total pressure combs; 2-2 Kulite dynamic pressure probes of exit; 3-3 exit total pressure combs; A-A Kulite dynamic static pressure sensors CH1 to CH4.

Fig. 1 Schematic layout of test rig

Table 1 Design parameters of tested compressor

Parameters	Value
Number of blades	17
Chord length/mm	80.54
Hub tip ratio	0.565
Aspect ratio	0.956
Clearance at blade tip/mm	0.9
Designed rotating speed/(r/min)	22000
Tangential speed at blade tip/(m/s)	409.85

The rotor rotates clockwise from forward-looking-aft. Inlet-air distortion of plugboard type with 50% blockage ratio was taken in the present experiment as a typical example. The plugboard was imporous, and it was positioned upstream at a distance of $2D$ from the rotor's leading edge. Six 5-hole total pressure combs

and eight 6-hole total pressure combs were evenly distributed in front of and behind the rotor, respectively. As shown in Fig. 2, four Kulite dynamic wall static pressure sensors were set up on the casing 15 mm in front of the rotor's leading edge at circumference evenly. The four Kulite dynamic wall static pressure sensors CH1 to CH4 were used to measure the stall inception and stall disturbances. Three Kulite dynamic total pressure probes were set up on the downstream position 40 mm away from the rotor's trailing edge in circumference evenly, and these probes were placed at 10%, 50% and 90% blade height respectively.

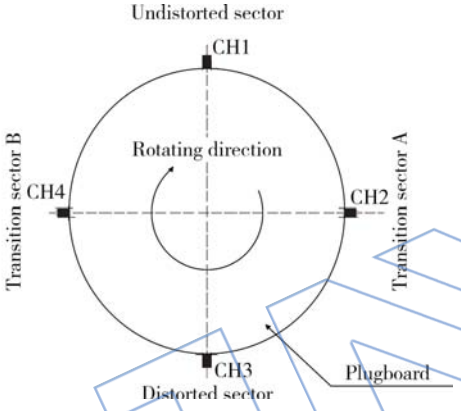

Fig. 2 Schematic of circumferential sectors in compressor

As shown in Fig. 2, for comparing the flowfields at different circumferential locations, the compressor was divided into four sectors: undistorted sector, transition sector A where the flow was rotating into the distortion sector, distorted sector and transition sector B where the flow was rotating out of the distortion sector. As shown in Fig. 3, five Kulite dynamic static pressure sensors CH4 to CH8 were set up in casing. By rotating the casing, the shock waves were measured in the four sectors. The effects of the performances and flow-field on transonic compressor's rotor were measured at 98% designed rotating speed under both distorted inlet and uniform inlet.

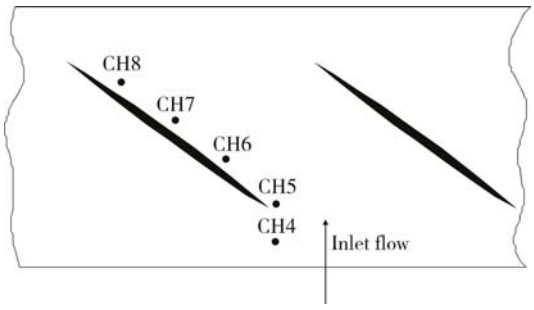

Fig. 3 Schematic of pressure sensors in axial direction

2 Results of experiment

2.1 Performance comparison

Characteristics were measured under uniform inlet and distorted inlet conditions. The measurements were repeated two times, and mean values were plotted in Fig. 4. The near stall point was acquired by suddenly-lowering of flowrate and total pressure ratio, which can be seen in Fig. 5(a). The data of Fig. 5(a) was obtained by successive acquisition. Fig. 5(b) is the signal from outlet dynamic total pressure sensors which are used to monitor the stall of the compressor. According to Fig. 5(a) and Fig. 5(b), the near stall point can be confirmed. A comparison of measured performances for uniform inlet and distorted inlet was given in Table 2. In

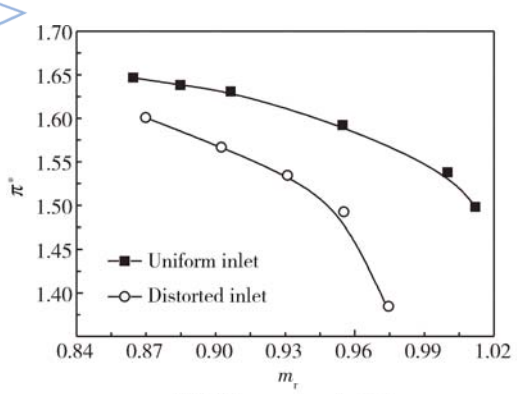

(a) Efficiency characteristics

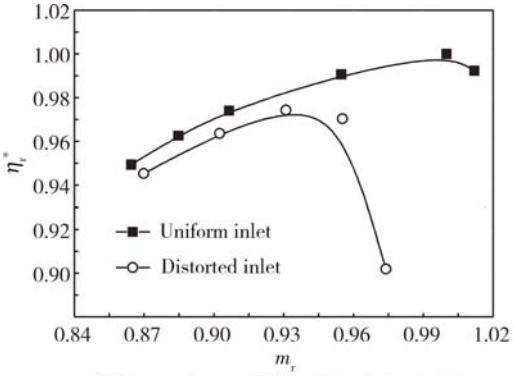

(b) Successive acquisition data of steady state

Fig. 4 Performance of compressor by experiment

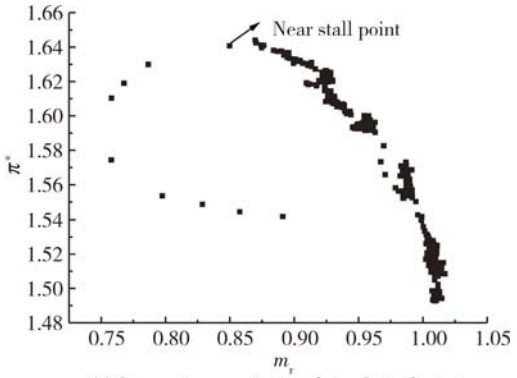

(a) Successive acquisition data of steady state

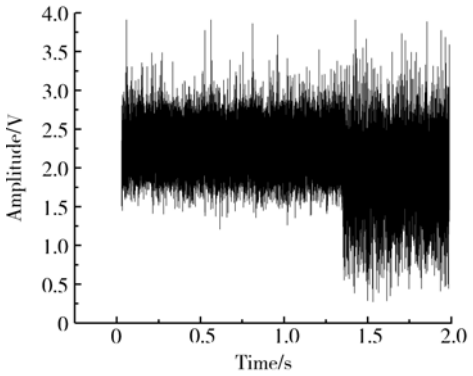

(b) Outlet dynamic total pressure of successive acquisition

Fig. 5 Judgement of near stall point

Fig. 4, the relative efficiency denotes the ratio of the measured efficiencies to the peak efficiency of uniform inlet condition, and the relative flowrates denote the ratio of the measured flowrate to the flowrate of solid casing at its peak efficiency. It can be seen from the experimental results that the performance of compressor decreases markedly under inlet-air distortion. The relative efficiency decreases 2.57%, and the stall margin decreases 6.05%.

Table 2 Comparison of performances under uniform inlet and distorted inlet

Casing type	$\eta^*_{\_peak}$/%	$\Delta\eta^*_{\_peak}$/%	M_s/%	ΔM_s/%
Uniform inlet	100	0	23.86	0
Distorted inlet	97.43	−2.57	17.81	−6.05

2.2 Phase change of total pressure distortion along compressor

Annulus numerical simulation that distorted parameters transfer along compressor was carried out on single stage and 3-stage compressor respectively[10-11] under pure circumferential total pressure distortion, and the result shows that the phase does not change when the total pressure distortion passes through the compressor. But, the circumferential total pressure distortion often accompanies rotating distortion in fact when combat aircraft flies at high angle-of-attack and high maneuverability. Therefore, the phase angle of the total pressure can change differently when the inlet total pressure distortion passes through the compressor's rotor.

By the method of interpolation to the data of inlet and outlet combs, the inlet and outlet total pressure contours were obtained respectively. The inlet and outlet total pressure contours which were obtained by experiment at the relative peak efficiency points are given in Fig. 6 and Fig. 7. Fig. 6 were obtained at uniform inlet,

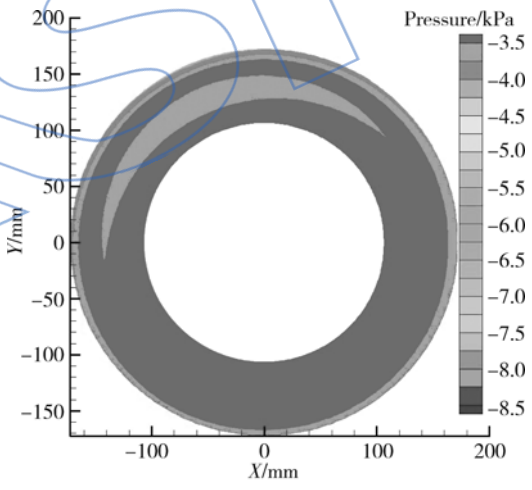

(a) Inlet

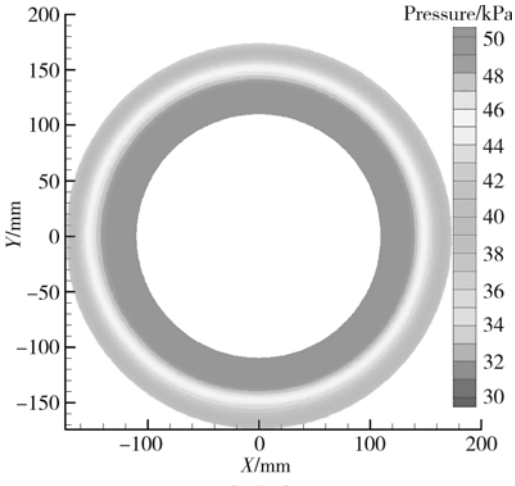

(b) Outlet

Fig. 6 Uniform inlet and outlet total pressure contours

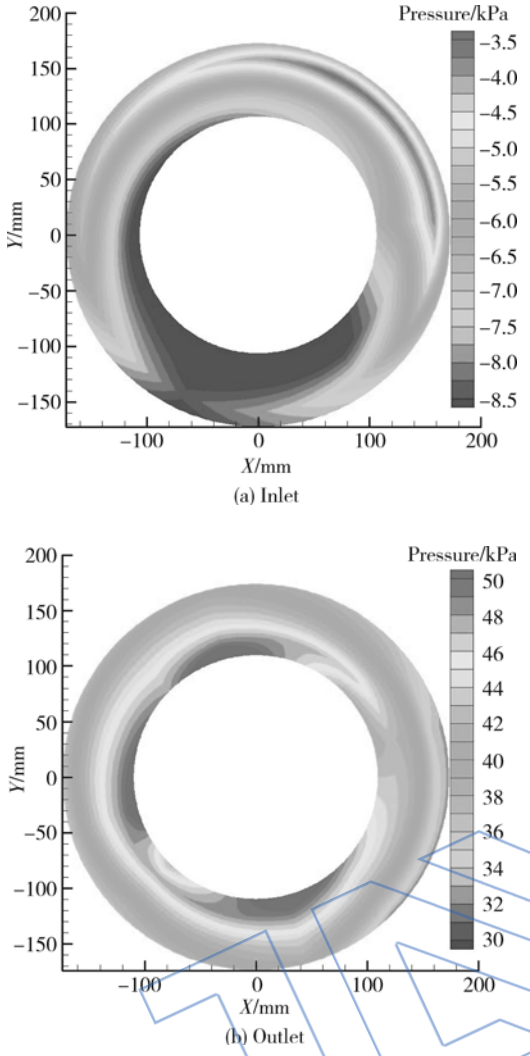

Fig. 7 Distorted inlet and outlet total pressure contours

and Fig. 7 were obtained at distorted inlet. From Fig. 7, it can be seen that the inlet-air distortion leads to the emergence of high pressure and low pressure regions at inlet. In addition, plugboard can generate a big vortex behind it. The existence of pressure difference and vortex leads to a pre-rotation of inlet flow. In order to demonstrate it, an unsteady numerical simulation was carried out. The equation solver was Numeca-Fine. The 3-D Reynolds averaged Navier-Stokes equations were solved by using the time propulsion method, and the physical time-step was 1.7×10^{-5} s. The turbulence model used Spalart-Allmaras, and the grid nodes were 4444529. The total temperature and total pressure of inlet were given. The back pressure of outlet was given at 50% blade height, and the back pressure of other blade height were solved by radial balance equations. The adiabatic and no-slip condition was used at solid boundary. From Fig. 8, it can be observed that inlet-air distortion leads to pre-rotation at the compressor's inlet, and furthermore, the inlet flow is positive pre-rotation and negative pre-rotation in transition sector A and transition sector B respectively, which is consistent with the conclusions of Refs. [12-13].

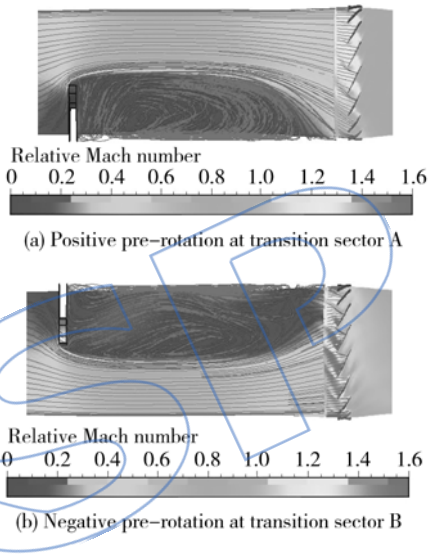

Fig. 8 Streamlines of absolute velocity at 90% blade height by numerical simulation

From Fig. 7, we can see the phase angle of the total pressure changes 90° when the inlet total pressure distortion passes through the compressor rotor. The reasons are that the pure circumferential total pressure distortion is simulated in Refs. [10-11], and the pre-rotating distortion caused by it is very weak. And when the plugboard is placed at the compressor's inlet, not only the circumferential inlet total pressure distortion is produced, but also, more importantly, as mentioned above, the stronger inlet rotating flow distortion would be produced. Because of pre-rotation of inlet flow, the relative velocity and angle-of-attack decreases and increases in transition sector A and transition sector B, respectively. So the shock wave is weaken and the work decreases in transition sector A, but the transition sector B is opposite. The strength of rotating flow in undistorted sector and distorted sector is weaker than that in the

transition sector, so there is still work from shock wave in these sectors. In conclusion, because of non-uniform distribution of shock waves, it causes non-uniform distribution of work at circumference. Therefore, compared with inlet total pressure, the phase angle of the outlet total pressure changes 90° under inlet-air distortion.

2.3 Shock wave distribution along circumference at peak efficient point

In order to analyze the shock wave distribution at circumference under inlet-air distortion, the dynamic wall static pressure was measured by experiment at four sectors. The blade passing frequency (BPF) was 6.3 kHz, and the frequency response of the dynamic pressure sensors was set up to 250 kHz, which can meet the test requirements fully. Fig. 9 and Fig. 10 are the maps of casing wall static pressure with relative flowrate $m_r = 0.931$ (corresponding to peak efficient point under inlet-air distortion). The data of Fig. 9 and Fig. 10 were obtained from the data on one time range of dynamic pressure sensors CH4 to CH8. As shown in Fig. 9, the pressure of transition sector A is lower than that of other three sectors, and the shock wave is not obviously, so the work of transition sector A is not generated by shock wave, and that of other three sectors are generated by shock wave. From the shock wave maps, it can be seen that the analysis about the transfer of total pressure distortion along compressor is correct. As shown in Fig. 9 and Fig. 10, the shock wave of uniform inlet is stronger than that of any distorted inlet in the same flowrate condition. The reason is that the incidence angle increases at transition sector B and decreases at transition sector A. So it causes separation in suction side at transition sector B, and separation in pressure side at transition sector A. In addition, the disturbances are enhanced obviously, and the flow becomes more chaos, so the mixing loss increases under inlet-air distortion. And the work addition ability decreases correspondingly.

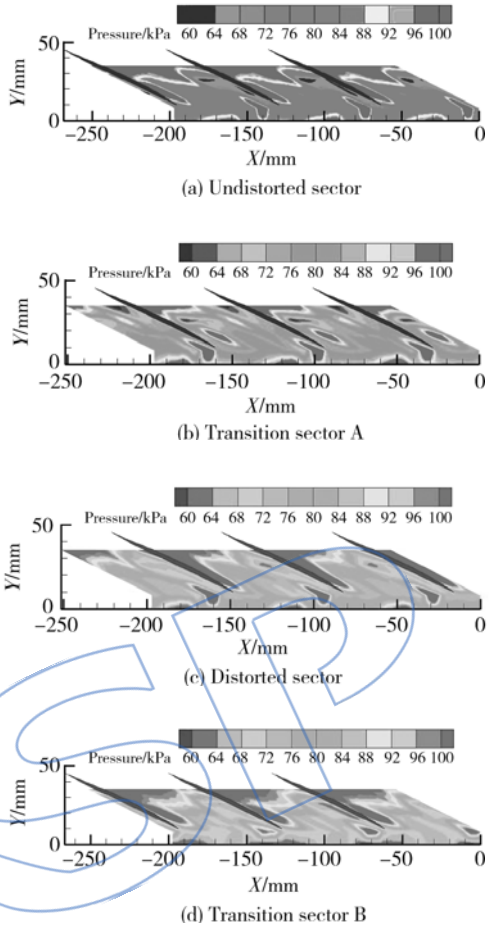

Fig. 9 Maps of casing wall static pressure of distorted inlet at four sectors by experiment

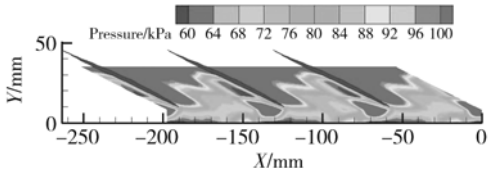

Fig. 10 Maps of casing wall static pressure of uniform inlet by experiment

2.4 Effect of inlet-air distortion on performance in four sectors at peak efficient point

The distribution of total pressure ratio along spanwise was analyzed in four sectors. The spanwise was the direction from hub to tip. The inlet total pressure was the average value of the six inlet combs. The outlet total pressure used the values of outlet combs in four sectors respectively. Each of outlet combs measured six pressures along spanwise.

From Fig. 11, for the uniform inlet, we can

see the total pressure ratio is even in circumference. For inlet distortion, positive pre-rotation in transition sector A would result in smaller relative velocity, leading to weaker shock wave and smaller input work, while the negative pre-rotation in transition sector B would result in larger relative velocity, leading to stronger shock wave. The two pre-rotating flows converge to distorted sector, and the flows tend to axial direction, so the pre-rotating flow decreases, and the axial flow increases, which leads to larger relative velocity and stronger shock wave in distorted sector. This is different from pure circumferential total pressure distortion. Hence, as shown in Fig. 12, the total pressure ratio in transition sector B and distorted sector increases while the total pressure ratio in transition sector A decreases.

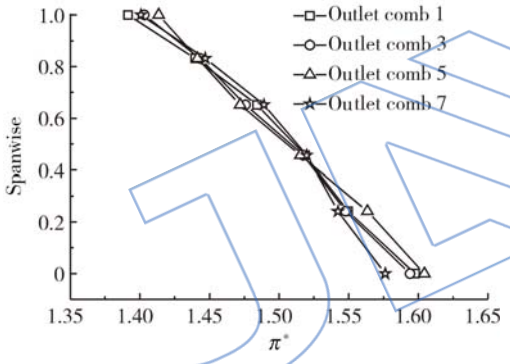

Fig. 11 Uniform inlet by experiment

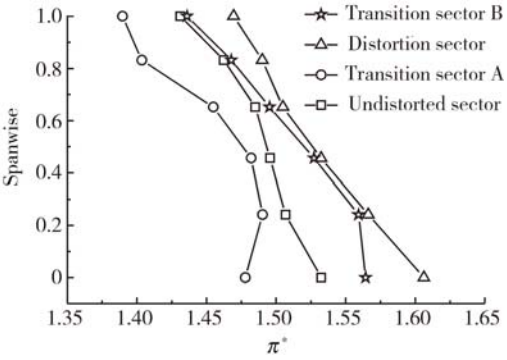

Fig. 12 Distorted inlet by experiment

2.5 Analysis of stall characteristics

The stall characteristics were captured by three outlet dynamic total pressure sensors and four inlet dynamic wall static pressure sensors. The dynamic total pressure sensors were placed at the position of 40 mm after the rotor's trailing edge in circumference evenly, and dynamic wall static pressure sensors were placed at the casing 15 mm in front of the rotor's leading edge at circumference evenly. The stall propagation in radial direction was measured by the outlet dynamic total pressure sensors, and the stall disturbances and stall inception were measured by inlet dynamic wall static pressure sensors.

2.5.1 Stall propagation in radial direction

The compressor enteres stall state when outlet dynamic total pressure signals emerge suddenly obvious periodic fluctuation, and the pressure values decrease. The stall characteristics measured at the compressor outlet are shown in Fig. 13. The figures are low-pass filtered by 300 Hz. As shown in Fig. 13, whether uniform inlet or distorted inlet, the stall types of the compressor are tip stall and abrupt stall. But, it is worth noting that the propagation of stall need only one revolution from tip to hub under uniform inlet, however it need three to four revolutions under distorted inlet. The results show that distorted inlet slowes down the abruption of stall disturbances. And JIANG et al.[14-15] also observed this similar phenomena on a low speed compressor.

2.5.2 Stall propagation at circumference

The stall types of the compressor are tip stall under uniform inlet and distorted inlet, so the stall disturbances and stall inception can be analyzed by measuring the dynamic wall static pressure of casing in front of the rotor.

The S transformation of pressure signals within one second is shown in Fig. 14. The horizontal ordinate is time, and the vertical coordinate is frequency, as well as the color depth denotes the size of amplitude. The rotor rotated about 360 revolutions per second at 98% rotating speed. As shown in Fig. 14, compared with uniform inlet, the frequency and amplitude of disturbances in front of rotor are increased under inlet-air distortion, and the disturbances

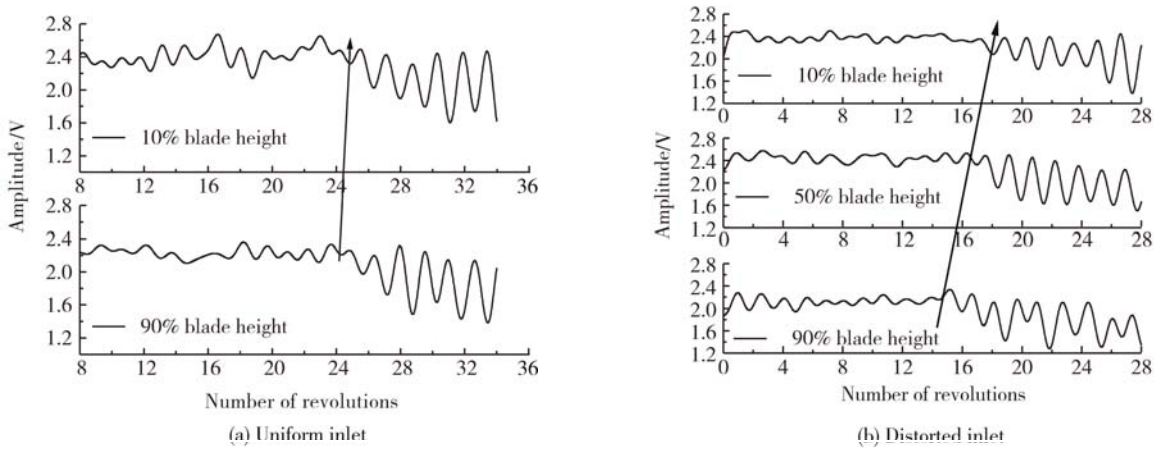

Fig. 13 Propagation of stall in radial direction

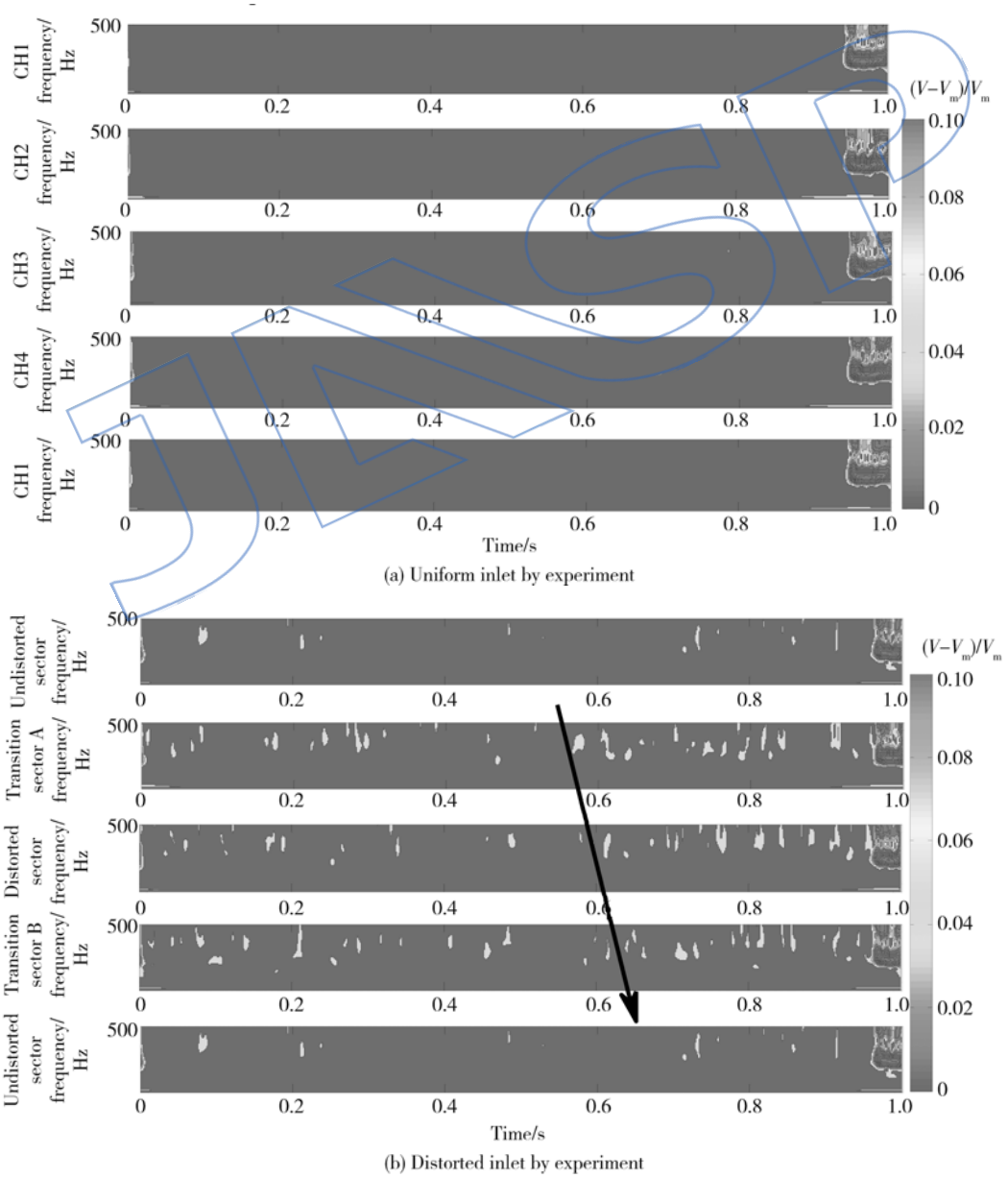

Fig. 14 Stall disturbances in front of rotor

of undistorted sector are weaker than ones of the other three sectors. In addition, the disturbances become strong suddenly within about 0.4 s in transition sectors and distorted sector under inlet-air distortion before the compressor stall. But, it is restrained by undistorted sector, so the compressor do not stall immediately. However the suddenly strong disturbances are the stall omen which leads to compressor stall in advance.

Fig. 15 shows the signals of dynamic wall static pressure in front of rotor. The signals are low-pass filtered by 300 Hz. The compressor enteres full stall state when the periodic and sharp pulse signals emerges. The stall process is recorded by Fig. 15. From the figure, it can be seen that the low amplitude stall disturbances always exist in front of the rotor before compressor stall, and the disturbances are the necessary conditions of the compressor stall. When the back pressure reaches a certain degree, the disturbances would develop into big stall cell quickly in about four revolutions, and cause whole compressor to stall.

The disturbances of distorted inlet are greater than ones of uniform inlet, which can lead to compressor stall in advance under inlet-air distortion. Because of the symmetry of uniform inlet, the compressor stall inception do not fix in certain position. The dash line arrows in Fig. 15 (b) and Fig. 15(c) indicate that the disturbances which are generated by a certain sector do not propagate in other sectors. The solid line arrows indicate that the next disturbance of the sector is enlarged gradually when it passes through the other three sectors, and it causes compressor stall quickly within two revolutions. As shown in Fig. 15(b) and Fig. 15(c), the position of stall inception is in transition sector A and transition sector B respectively. By repeating experiments four times, the results show that the position of stall inception is always in transition sector A or transition sector B under inlet-air distortion. Therefore, the conclusion that the position of compressor stall inception is in transition sectors under inlet-air distortion can be drawn. As already mentioned, the separation of transition sectors is most severe, and the disturbances are strengthened under inlet-air distortion. Therefore, it causes stall firstly in one of transition sectors under inlet-air distortion.

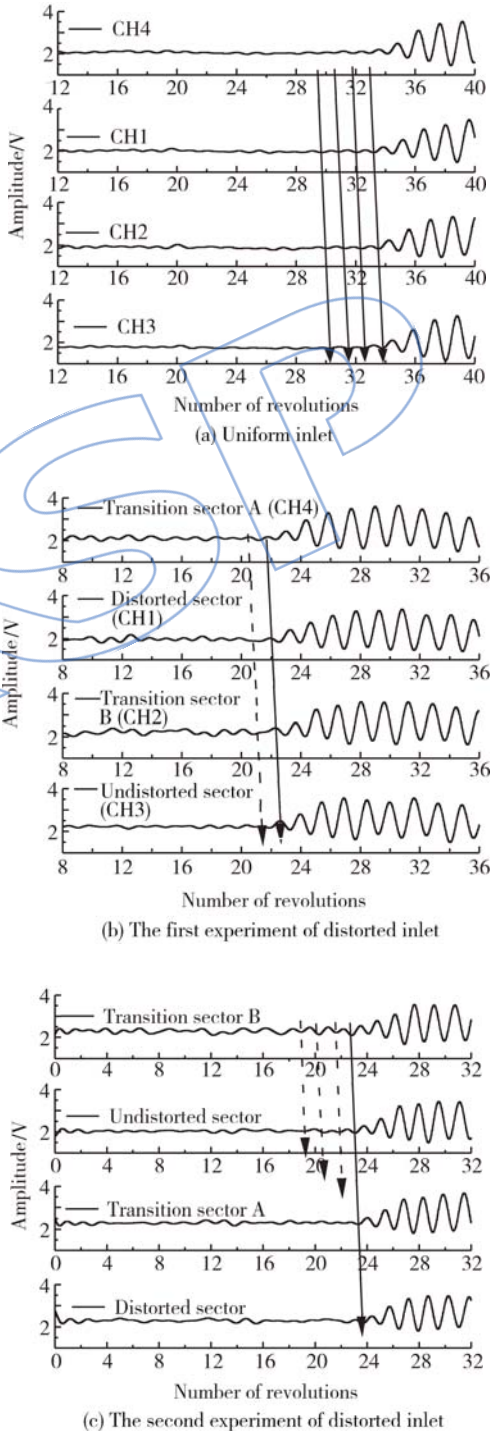

Fig. 15 Propagation of disturbances in circumferential direction

3 Conclusion

The mechanism of performance degradation and the flow field characteristics were analyzed in detail on a transonic compressor under inlet-air distortion. From the experimental results and analysis, the following conclusion can be drawn.

1) The pre-rotation which is caused by inlet-air distortion leads to non-uniform distribution of shock waves at circumference, which causes non-uniform distribution of work. Therefore, the phase angle of the total pressure changes 90° when the inlet total pressure distortion passes through compressor rotor.

2) The flow loss of inlet-air distortion is much larger than that of uniform inlet, which makes the efficiency of compressor decrease markedly in the whole range of flowrate under inlet-air distortion.

3) The disturbances of compressor inlet are enhanced markedly under inlet-air distortion, which is the main reason to induce instability of compressor in advance.

4) The stall inception position of transonic compressor is uncertain under uniform inlet, but the stall inception position is always in transition sectors under distorted inlet.

Acknowledgments

The authors are grateful to Doctor WANG Zhuoqi and Master GAN Lu for their selfless help.

References:

[1] Harry D P, Lubick R J. Inlet-air distortion effects on stall, surge and acceleration margin of a turbojet engine equipped with variable compressor inlet guide vanes[R]. NACA RM E54K26, 1955.

[2] Malker C, Sivo J N, Jansen E T. Effects of unequal air-flow distribution from twin inlet ducts on performance of an axial-flow turbojet engine[R]. NACA RM E54E13, 1954.

[3] Hermanson K, Thole K. Effect of non-uniform inlet conditions on endwall secondary flow[J]. Journal of Turbomachinery, 2002, 124(10): 623-631.

[4] Hirai K, Kodama H, Nozaki O, et al. Unsteady three-dimensional analysis of inlet distortion in turbomachinery [R]. AIAA 1997-2735, 1997.

[5] Hah C, Rabe D, Sullivan T, et al. Effects of inlet distortion on the flow field in a transonic compressor rotor[J]. Journal of Turbomachinery, 1998, 120(2): 233-246.

[6] Doyle M, Dixon S, Horlock J. Circumferential asymmetry in axia flow compressors[J]. Journal of the Royal Aeronautical Soeiety, 1966, 70(10): 956-963.

[7] Greitzer E. Surge and rotating stall in axial flow compressors: Part Ⅰ theoretical compression system model[J]. Journal of Engineering for Power, 1976, 98(2): 201-213.

[8] Stenning A. Inlet distortion effects in axial compressors [J]. Fluids Engineering, 1980, 102(1): 7-13.

[9] Chue R, Hynes T, Greitzer E, et al. Calculation of inlet distortion induced compressor flow field instability[J]. Journal of Heat and Fluid Flow, 1989, 10(3): 211-223.

[10] YAO Jixian, Steven E, Aspi R. High-fidelity numerical analysis of per-rev-type inlet distortion trasfer in mutistage fans: Part Ⅰ simulations with selected blade rows[R]. ASME Paper GT-2008-50812, 2008.

[11] YAO Jixian, Steven E, Aspi R. High-fidelity numerical analysis of per-rev-type inlet distortion trasfer in mutistage fans: Part Ⅱ entire component simulation and investigation [R]. ASME Paper GT-2008-50813, 2008.

[12] LI Maoyi, LU Yajun, GONG Zhiqiang. PIV investigation of the internal flow in an axial flow compressor rotor under inlet distortion[J]. Journal of Aerospace Power, 2006, 21(3): 461-466. (in Chinese)

[13] LI Maoyi, YUAN Wei, SONG Xizhen, et al. An experimental investigation about the effect of the partial treatment on a transonic axial-flow compressor performance under inlet distortion [R]. ASME Paper GT-2012-68442, 2012.

[14] JIANG Huabing. Experimental investigation on the unsteady cooperative flow control for the compressor with inlet distortion[D]. Beijing: Beijing University of Aeronautics and Astronautics, 2008. (in Chinese)

[15] JIANG Huabing, LU Yajun, YUAN Wei, et al. Experimental investigation of the influence of inlet distortion on the stall inception in a low speed axial compressor[R]. ASME Paper GT-2009-59139, 2009.